JOM, Vol. 74, No. 2, 2022
https://doi.org/10.1007/s11837-021-04870-0

Experimental Study on the Phase Relations of the SiO_2-MgO-TiO_2 System in Air at 1500°C

MIN CHEN [1,4,5] XINGBANG WAN [1,6] JUNJIE SHI [2,3,7] PEKKA TASKINEN [1,8] and ARI JOKILAAKSO [1,9]

1.—Department of Chemical and Metallurgical Engineering, School of Chemical Engineering, Aalto University, Kemistintie 1F, P.O. Box 16100, 00076 Aalto, Finland. 2.—School of Metallurgy, Northeastern University, Shenyang 110819, China. 3.—Key Laboratory for Ecological Metallurgy of Multimetallic Minerals (Ministry of Education), Northeastern University, Shenyang 110819, China. 4.—e-mail: minchen0901@hotmail.com. 5.—e-mail: min.chen@aalto.fi. 6.—e-mail: xingbang.wan@aalto.fi. 7.—e-mail: junjieshi@126.com. 8.—e-mail: pekka.taskinen@aalto.fi. 9.—e-mail: ari.jokilaakso@aalto.fi

We investigated the phase relations of the SiO_2-MgO-TiO_2 system in air at 1500°C using the high-temperature isothermal equilibration/quenching technique, followed by x-ray diffraction measurements and direct phase analysis using scanning electron microscopy coupled with x-ray energy dispersive spectrometry. One single liquid phase domain, five two-phase domains (liquid-TiO_2, liquid-cristobalite, liquid-MgO·SiO_2, liquid-2MgO·SiO_2, and liquid-MgO·2TiO_2), and five three-phase regions (liquid-TiO_2-MgO·2TiO_2, liquid-MgO·SiO_2-cristobalite, liquid-TiO_2-cristobalite, liquid-MgO·SiO_2-2MgO·SiO_2 and liquid-2MgO·SiO_2-MgO·2TiO_2) were observed. We constructed a 1500°C isothermal phase diagram based on the experimentally measured liquid compositions. We compared simulations using MTDATA and FactSage thermodynamic software and their databases with the experimental results obtained in this study. These results can be used to provide guidelines for updating the MTDATA and FactSage titania-bearing thermodynamic databases by reassessing the thermodynamic properties of the phase with new experimental data.

INTRODUCTION

With the steady growth in the generation of blast furnace slags from vanadium-titanium magnetite ores, the recovery of titania from industrial titania-bearing slags containing 22–25 wt.% TiO_2[1–3] is attracting increasing attention.[3–15] Over the past decades, both hydrometallurgical and pyrometallurgical methods[15–24] for processing titania-bearing slags have been applied and investigated intensively. Recently, a selective crystallization method and separation of a titania-enriched phase has also been proposed[25–27] to collect titania into a certain phase. For all these pyrometallurgical methods, the recovery of titanium is closely correlated with the thermodynamic behavior of titania in high-temperature slag systems. The formation of titania-rich minerals can be estimated and their fractions evaluated using the phase equilibrium information of the system.

Based on their composition, industrial titania-bearing slags[1,21,28] conform to the Al_2O_3-CaO-SiO_2-MgO-TiO_2-Ti_2O_3 system.[29] The phase relations of the Al_2O_3-CaO-SiO_2-MgO-TiO_2 system have been intensively investigated under varying conditions[27,29–42] by using different thermodynamic modeling tools and experimental methods. These studies provide guidance for the selective crystallization of rutile (TiO_2), perovskite (CaO·TiO_2), and pseudobrookite ($MgTi_2O_5$-Al_2TiO_5) phases. Recently, the phase equilibria of the CaO-SiO_2-TiO_2-10 wt.% Al_2O_3 quasi-ternary system were investigated in air at 1300–1600°C by Wang et al.[43] and Chen et al.[44] They constructed isotherms for the rutile and perovskite primary phase fields.[43,44] However,

(Received April 28, 2021; accepted August 23, 2021; published online September 21, 2021)

Table I. Materials used for preparing the slags

Materials	Purity/wt.%	Supplier
SiO_2	99.995	Alfa Aesar (Kandel, Germany)
MgO	99.95	Alfa Aesar (Karlsruhe, Germany)
TiO_2	99.8	Sigma-Aldrich (Steinheim, Germany)

the experimental data for the low-order binary/ternary systems are the key for the reliable thermodynamic modeling of high-order systems. Therefore, it is important to update the experimental thermodynamic data for the low-order systems.

The phase relations of the CaO-TiO_2,[45,46] MgO-TiO_2,[47–50] SiO_2-TiO_2,[51–55] and Al_2O_3-TiO_2[52,56–60] binary systems have been investigated intensively. However, limited effort has been devoted to the TiO_2-bearing ternary systems, i.e., CaO-SiO_2-TiO_2,[61–64] CaO-Al_2O_3-TiO_2,[65,66] CaO-MgO-TiO_2,[67] SiO_2-Al_2O_3-TiO_2,[68,69] and Al_2O_3-MgO-TiO_2.[70,71] Regarding the SiO_2-MgO-TiO_2 system, Massazza and Sirchia[72] carried out the first study on determining the liquidus of the system in 1957 at 1500–1700°C. The detailed experimental procedures were not reported in their paper. Moreover, a loss due to volatilization of SiO_2 has been found for mixtures rich in silica and melted at high temperatures, which might cause inaccuracies for the determined phases. MacGregor[73] determined the liquidus and solidus relationships in the Mg_2SiO_4-$MgSiO_3$-TiO_2-$MgTi_2O_5$ domain of the MgO-SiO_2-TiO_2 system at 1500–1900°C. Hermann et al.[74] measured the solubility of TiO_2 in olivine in the MgO-SiO_2-TiO_2 system under conditions of atmospheric pressure at 1200–1500°C, but without illustrating the liquid domain. They reported that the highest solubility of TiO_2 was obtained when the olivine was equilibrated with spinel ($2MgO{\cdot}TiO_2$).[74] Yan et al.[75] determined the phase equilibria of the SiO_2-MgO-TiO_x quasi-ternary system under reducing atmospheres at 1600°C. The isothermal SiO_2-MgO-TiO_x phase diagram at P_{O2} of 4.85×10^{-11} atm was constructed and the effect of P_{O2} on the phase relations was demonstrated by comparison with the results by Massazza and Sirchia.[72] Moreover, the isotherms of the anosovite primary phase field were also determined at P_{O2} of 1.94×10^{-9} and 2.75×10^{-13} atm, suggesting that the solubility of TiO_x in the liquid phase decreased with decreasing P_{O2}.

In summary, the SiO_2-MgO-TiO_2 system was either not systematically investigated or there are significant discrepancies between the already existing studies. Therefore, the purpose of the present study was to investigate the phase relations in the SiO_2-MgO-TiO_2 system in air at 1500°C to resolve the current existing contradictions and to provide experimentally reliable, fundamental thermodynamic data for the thermodynamic assessment of the CaO-SiO_2-MgO-Al_2O_3-TiO_2 system. The results are expected to provide guidance for the selective crystallization of TiO_2 and $MgO{\cdot}2TiO_2$ phases from the slags by modifying the composition of industrial titania-bearing blast furnace slags.

EXPERIMENTAL

The starting materials used for synthesizing the slags are listed in Table I. Each powder was weighed in a certain ratio based on the designed composition and mixed thoroughly in an agate mortar before being pressed into a pellet using a hydraulic press with a force of 5 metric tons.

The experiments were followed by high-temperature isothermal equilibration, quenching, and direct phase analysis by applying the XRD and SEM-EDS techniques. A vertical alumina tube furnace (Nabertherm, RHTV 40-250/18, Germany) was used for the high-temperature equilibration experiments, as shown in Fig. 1. Synthetic slag (0.15–0.3 g) was pre-heated at 1600°C for 30 min and then equilibrated at 1500°C for each experiment. A pure platinum foil was used for making crucibles to support the sample pellet. A platinum wire inserted into the furnace from the top end of the guiding tube was used to hold the crucibles. The sample temperature was monitored by an alumina-shielded S-type Pt/90%Pt-10%Rh thermocouple placed next to the sample. The samples were annealed at 1500°C for equilibration, and then quenched in an ice-water mixture to retain the phase assemblies from a high temperature.[76,77] The detailed experimental procedures used were described in our previous studies.[32–34,44,64]

The quenched samples were dried at room temperature, and part of the sample was mounted in epoxy resin, then ground and polished using a metallographic polishing cloth with diamond sprays. The polished sample surfaces were carbon-coated using a LEICA EM SCD50 sputtering device (Leica Mikrosysteme, Austria). A Tescan MIRA 3 scanning electron microscope (SEM, Tescan, Brno, Czech Republic) equipped with an UltraDry silicon drift energy dispersive X-ray spectrometer (EDS, Thermo Fisher Scientific, Waltham, MA, USA) and NSS microanalysis software were used to measure the equilibrium phase compositions. An accelerating voltage of 15 kV, beam current of 20 nA, and a working distance of 20 mm were adopted for the SEM-EDS analysis. The standards and analyzed X-ray lines in the EDS analysis were as follows: quartz

Table II. Equilibrium phase compositions for the SiO_2-MgO-TiO_2 system in air at 1500°C

Sample	Initial compositions/wt.%			Equilibrium phases	Equilibrium compositions/wt.%		
	TiO_2	SiO_2	MgO		TiO_2	SiO_2	MgO
Single liquid							
C1	44.92	33.23	21.84	Liquid	45.9 ± 0.9	33.5 ± 0.5	20.5 ± 0.4
C68	10.07	55.81	34.12	Liquid	10.2 ± 0.1	57.0 ± 0.1	32.7 ± 0.1
C69	12.47	52.91	34.62	Liquid	12.8 ± 0.1	53.9 ± 0.1	33.3 ± 0.1
C70	15.2	50.15	34.65	Liquid	15.3 ± 0.1	51.5 ± 0.1	33.2 ± 0.1
C71	17.7	47.79	34.51	Liquid	17.8 ± 0.1	49.0 ± 0.1	33.2 ± 0.1
C75	38.03	35.11	26.86	Liquid	37.8 ± 0.1	35.8 ± 0.1	26.4 ± 0.1
Liquid + TiO_2							
C5	57.77	23.44	18.79	Liquid	49.3 ± 1.0	28.5 ± 0.6	22.3 ± 0.4
				TiO_2	99.7 ± 0.0(4)	0.2 ± 0.0(3)	0.1 ± 0.0(2)
C43	48.57	30.14	21.29	Liquid	47.1 ± 0.2	32.4 ± 0.2	20.6 ± 0.1
				TiO_2	99.8 ± 0.0(4)	0.2 ± 0.0(2)	0.1 ± 0.0(2)
C44	47.92	32.36	19.72	Liquid	46.9 ± 0.2	33.2 ± 0.4	20.0 ± 0.4
				TiO_2	99.8 ± 0.0(2)	0.2 ± 0.0(3)	0.1 ± 0.0(2)
Liquid + cristobalite							
C46	30	50	20	Liquid	36.2 ± 0.1	41.0 ± 0.2	22.8 ± 0.12
				Cristobalite	3.1 ± 0.1	96.9 ± 0.1	0.0(3) ± 0.0(2)
C47	26.73	52.64	20.63	Liquid	33.2 ± 0.2	42.8 ± 0.2	24.0 ± 0.1
				Cristobalite	2.8 ± 0.1	97.2 ± 0.1	0.0(3) ± 0.0(2)
C48	22.37	55.72	21.91	Liquid	27.0 ± 0.2	46.8 ± 0.1	26.2 ± 0.1
				Cristobalite	2.4 ± 0.1	97.6 ± 0.1	0.0(2) ± 0.0(2)
C49	17.58	59.1	23.32	Liquid	22.2 ± 0.1	50.3 ± 0.2	27.5 ± 0.1
				Cristobalite	2.1 ± 0.1	97.9 ± 0.1	0.0(2) ± 0.0(2)
C50	12.91	62.59	24.5	Liquid	16.6 ± 0.1	53.8 ± 0.1	29.6 ± 0.1
				Cristobalite	1.6 ± 0.1	98.3 ± 0.1	0.0(1) ± 0.0(1)
C51	8.87	65.43	25.7	Liquid	11.2 ± 0.1	57.3 ± 0.2	31.5 ± 0.2
				Cristobalite	1.1 ± 0.0(4)	98.8 ± 0.0(3)	0.0(3) ± 0.0(2)
C53	36.27	45.77	17.96	Liquid	43.9 ± 0.2	35.7 ± 0.2	20.5 ± 0.1
				Cristobalite	3.6 ± 0.2	96.4 ± 0.2	0.0(3) ± ± 0.0(1)
Liquid + MgO·SiO_2							
C73	8.8	56.64	34.56	Liquid	10.4 ± 0.1	57.2 ± 0.1	32.4 ± 0.0(4)
				MgO·SiO_2	0.6 ± 0.1	60.1 ± 0.1	39.2 ± 0.0(4)
Liquid + 2MgO·SiO_2							
C58	15.04	48.02	36.94	Liquid	16.5 ± 0.1	49.3 ± 0.1	34.3 ± 0.1
				2MgO·SiO_2	0.2 ± 0.1	44.3 ± 0.1	55.5 ± 0.1
C59	18.99	43.05	37.96	Liquid	21.7 ± 0.1	44.5 ± 0.1	33.8 ± 0.1
				2MgO·SiO_2	0.2 ± 0.1	44.4 ± 0.1	55.3 ± 0.1
C60	25.02	38.37	36.61	Liquid	30.3 ± 0.1	36.9 ± 0.1	32.8 ± 0.1
				2MgO·SiO_2	0.3 ± 0.1	43.9 ± 0.1	55.8 ± 0.1
C61	30.14	33.37	36.49	Liquid	36.0 ± 0.2	32.3 ± 0.1	31.7 ± 0.2
				2MgO·SiO_2	0.4 ± 0.1	43.5 ± 0.1	56.1 ± 0.1
C78	22.98	40.5	36.52	Liquid	25.3 ± 0.1	41.4 ± 0.1	33.3 ± 0.1
				2MgO·SiO_2	0.2 ± 0.1	44.6 ± 0.1	55.2 ± 0.1
Liquid + MgO·2TiO_2							
C65	51.92	22.98	25.1	Liquid	45.6 ± 0.3	28.8 ± 0.2	25.6 ± 0.1
				MgO·2TiO_2	79.6 ± 0.1	0.5 ± 0.0(4)	20.0 ± 0.1
C66	51.88	20.63	27.49	Liquid	44.0 ± 0.1	27.2 ± 0.1	28.9 ± 0.1
				MgO·2TiO_2	79.5 ± 0.3	0.5 ± 0.0(4)	20.0 ± 0.3
Liquid + TiO_2 + MgO·2TiO_2							
C7	62.45	18.69	18.86	Liquid	50.3 ± 0.3	27.3 ± 0.4	22.4 ± 0.3
				TiO_2	99.7 ± 0.0(4)	0.2 ± 0.0(3)	0.1 ± 0.0(2)
				MgO·2TiO_2	79.8 ± 0.1	0.5 ± 0.0(3)	19.7 ± 0.1
C11	67.17	13.35	19.48	Liquid	51.3 ± 0.3	26.4 ± 0.2	22.3 ± 0.3
				TiO_2	99.7 ± 0.1	0.2 ± 0.0(3)	0.1 ± 0.0(2)
				MgO·2TiO_2	79.7 ± 0.3	0.4 ± 0.0(3)	19.8 ± 0.3
Liquid + cristobalite + MgO·SiO_2							
C52	5.35	67.92	26.73	Liquid	10.2 ± 0.2	58.0 ± 0.2	31.8 ± 0.1
				Cristobalite	0.9 ± 0.1	99.0 ± 0.1	0.0(4) ± 0.1
				MgO·SiO_2	0.6 ± 0.1	60.2 ± 0.1	39.2 ± 0.1

Table II. continued

Sample	Initial compositions/wt.%			Equilibrium phases	Equilibrium compositions/wt.%		
	TiO_2	SiO_2	MgO		TiO_2	SiO_2	MgO
C54	4.29	62.09	33.62	Liquid	9.8 ± 0.2	58.6 ± 0.2	31.7 ± 0.1
				Cristobalite	0.9 ± 0.2	99.1 ± 0.2	0.0(2) ± 0.0(3)
				MgO·SiO_2	0.5 ± 0.1	60.6 ± 0.1	38.9 ± 0.1
C55	5.88	58.45	35.67	Liquid	9.4 ± 0.2	58.7 ± 0.2	31.9 ± 0.1
				Cristobalite	1.0 ± 0.1	99.0 ± 0.1	0.0(3) ± 0.0(2)
				MgO·SiO_2	0.5 ± 0.1	60.4 ± 0.1	39.1 ± 0.1
Liquid + TiO_2 + cristobalite							
C45	42.89	43.14	13.97	Liquid	46.6 ± 0.3	33.7 ± 0.3	19.6 ± 0.1
				TiO_2	99.8 ± 0.0(2)	0.2 ± 0.0(2)	0.1 ± 0.0(2)
				Cristobalite	4.0 ± 0.5	96.0 ± 0.5	0.0(1) ± 0.0(2)
Liquid + MgO·SiO_2 + 2MgO·SiO_2							
C57	10.13	52.76	37.11	Liquid	11.5 ± 0.1	53.6 ± 0.1	34.9 ± 0.1
				MgO·SiO_2	0.6 ± 0.1	60.3 ± 0.2	39.1 ± 0.2
				2MgO·SiO_2	0.2 ± 0.1	44.2 ± 0.1	55.6 ± 0.1
Liquid + 2MgO·SiO_2 + MgO·2TiO_2							
C72	45.43	20.99	33.58	Liquid	42.0 ± 0.2	26.7 ± 0.2	31.3 ± 0.1
				2MgO·SiO_2	0.6 ± 0.1	43.9 ± 0.1	55.5 ± 0.1
				MgO·2TiO_2	79.4 ± 0.1	0.4 ± 0.0(4)	20.2 ± 0.1

(for O-Kα and Si-Kα), rutile (for Ti-Kα), and pure metals Mg (for Mg-Kα). At least ten points were randomly measured for each phase to ensure its homogeneity and high statistical reliability. The Proza (Phi-Rho-Z) online matrix correction program[78] was employed for raw data processing before normalizing the results. The remaining sample was ground thoroughly in an agate mortar and then analyzed by x-ray diffraction [XRD, PANalytical X'Pert Powder XRD (alpha-1), the Netherlands] using Cu Kα radiation (40 kV, 40 mA). The XRD patterns were scanned over the range of 10° to 90° (2θ).

RESULTS AND DISCUSSION

Determination of the Equilibration Time and Valence State of Titanium

To determine the time required for getting both homogeneous liquid and solid phase compositions, a sample with an initial high silica concentration (22.37 wt.% TiO_2-55.72 wt.% SiO_2-21.91 wt.% MgO) was annealed at 1500°C for 2 h, 4 h, 8 h, and 12 h. Theoretically, a high silica concentration with a rigid silicon-oxygen network and high viscosity results in much slower mass transfer than relatively low silica concentrations.[79,80] Therefore, we used a sample with an initial high silica concentration for the time series. We decided that equilibration had been achieved based on the stabilization of the TiO_2, SiO_2, and MgO concentrations in the liquid phase as well as the SiO_2 and TiO_2 concentrations in solid cristobalite, as shown in Fig. 2a. It can be observed that equilibration in the present system was achieved in 8 h. However, with the purpose of ensuring sufficient growth of crystals, all samples were annealed at the experimental temperature for 12 h.

As is known, the element titanium exists as Ti^{4+}, Ti^{3+}, and Ti^{2+}, depending on the prevailing oxygen partial pressure and temperature. Therefore, it was critical to identify the valence state of Ti in the samples of the present study. Based on the prediction of the Ti-O stability phase diagram,[34,44,64] we found that the predominant form for titanium oxide was TiO_2 under the present experimental conditions of air ($\log_{10}P_{O2}$ of − 0.6778) at 1500°C. Pure TiO_2 was calcined in air at 1500°C for 24 h to verify the theoretical prediction. The XRD pattern for the calcined pure TiO_2 is shown in Fig. 2b, indicating that pure TiO_2 cannot be reduced to the lower valence states under the present experimental conditions. In our previous studies,[81,82] the oxidation state of Ti was also examined by XPS and it was proved that titanium existed in the samples as Ti^{4+}. Thus, it can be concluded that Ti^{4+} is the predominant stable valence state for titanium in all samples of the present study. Subsequently, the titanium oxide is presented as TiO_2 in the following sections.

Phase Relations at 1500°C

The equilibrium phase compositions, typical microstructures, and their corresponding XRD patterns are shown in Table II, Figs. 3, and 4, respectively. We observed one homogeneous single liquid domain, five liquid-solid two-phase coexistence domains (i.e., liquid-TiO_2, liquid-cristobalite, liquid-MgO·SiO_2, liquid-2MgO·SiO_2, and liquid-MgO·2TiO_2), and five liquid-solid-solid three-phase coexisting regions (i.e., liquid-TiO_2-cristobalite,

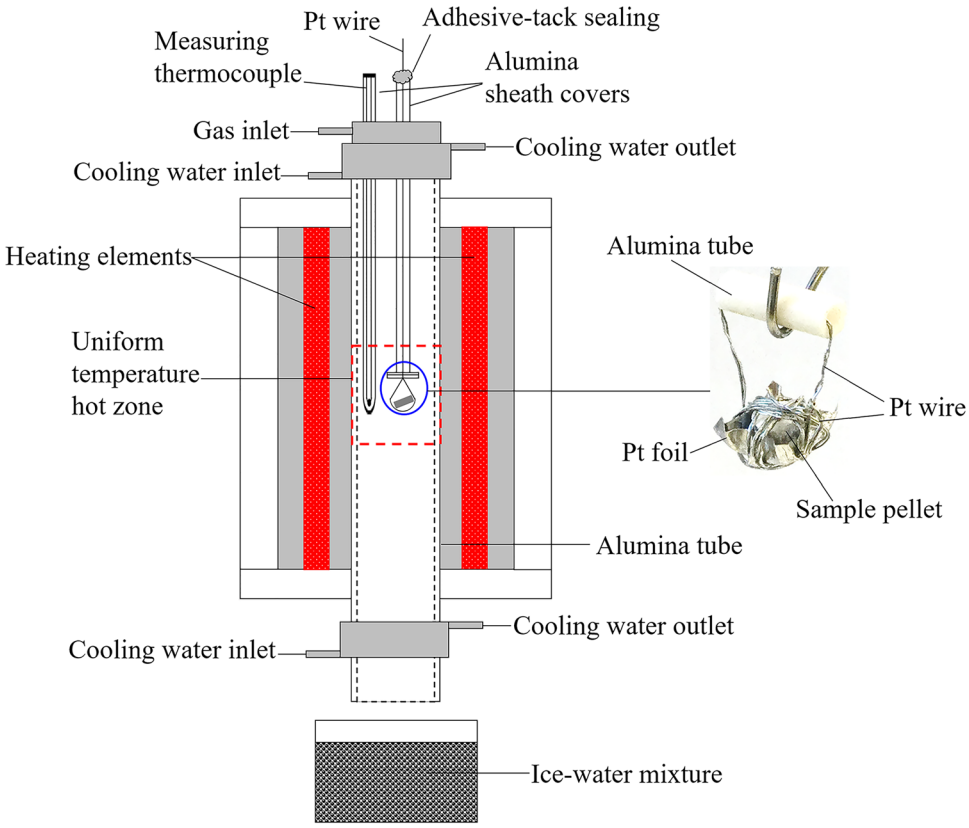

Fig. 1. Schematic cross section of experimental furnace with hanging sample pellet at its geometric center.

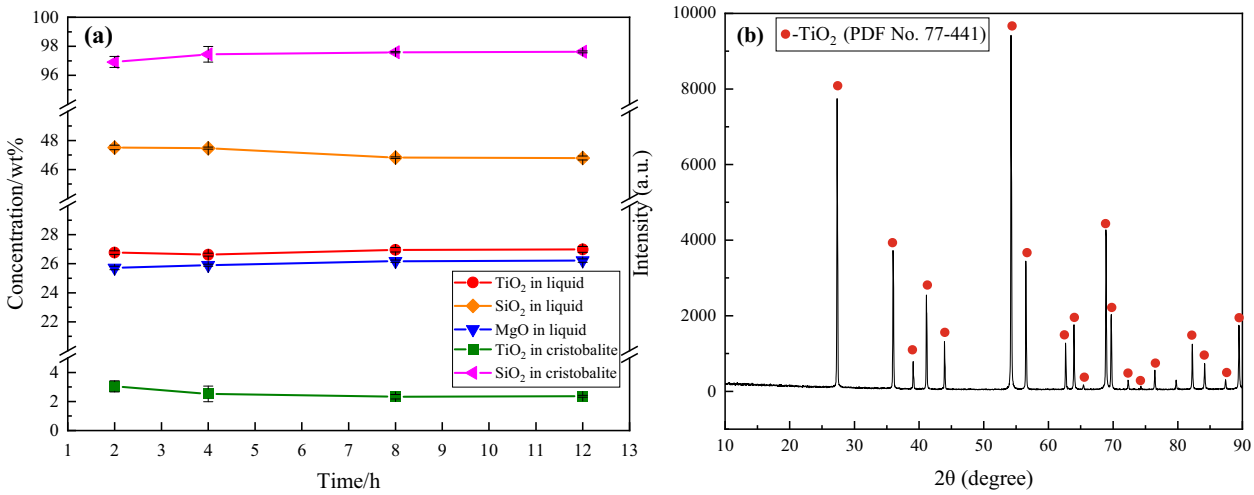

Fig. 2. TiO_2, SiO_2, and MgO concentrations in liquid oxide as well as TiO_2 and SiO_2 concentrations in solid cristobalite vs equilibration time (a); and XRD pattern of pure TiO_2 calcined at 1500°C for 24 hours (b).

liquid-$MgO{\cdot}SiO_2$-cristobalite, liquid-$MgO{\cdot}SiO_2$-$2MgO{\cdot}SiO_2$, liquid-$2MgO{\cdot}SiO_2$-$MgO{\cdot}2TiO_2$, and liquid-$MgO{\cdot}2TiO_2$-TiO_2). It should be noted that in the XRD pattern for sample C5 for liquid-TiO_2 two-phase equilibrium, there are several unindexed peaks with relatively low intensities, which may have been caused by the introduction of contaminants during the preparation of powder samples for XRD analysis. To demonstrate the reliability of EDS for determining the phase compositions, the measured TiO_2 results were compared with its theoretical value. The deviation between the theoretical

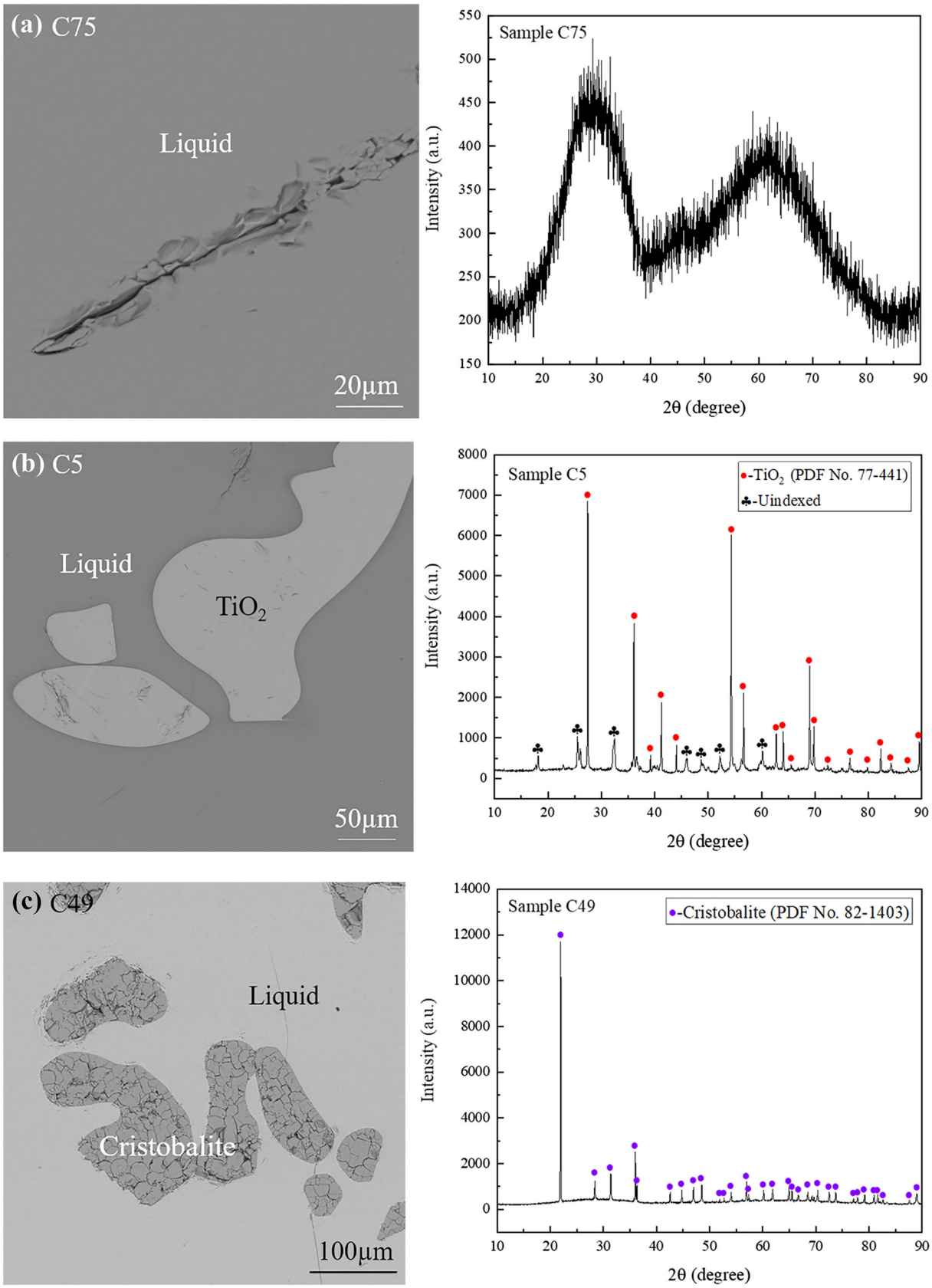

Fig. 3. Back scattered electron images and XRD patterns for single liquid phase equilibrium and liquid-solid two-phase coexisting equilibria; (a) single liquid; (b) liquid-TiO_2; (c) liquid-cristobalite; (d) liquid-MgO·SiO_2; (e) liquid-2MgO·SiO_2; and (f) liquid-MgO·2TiO_2.

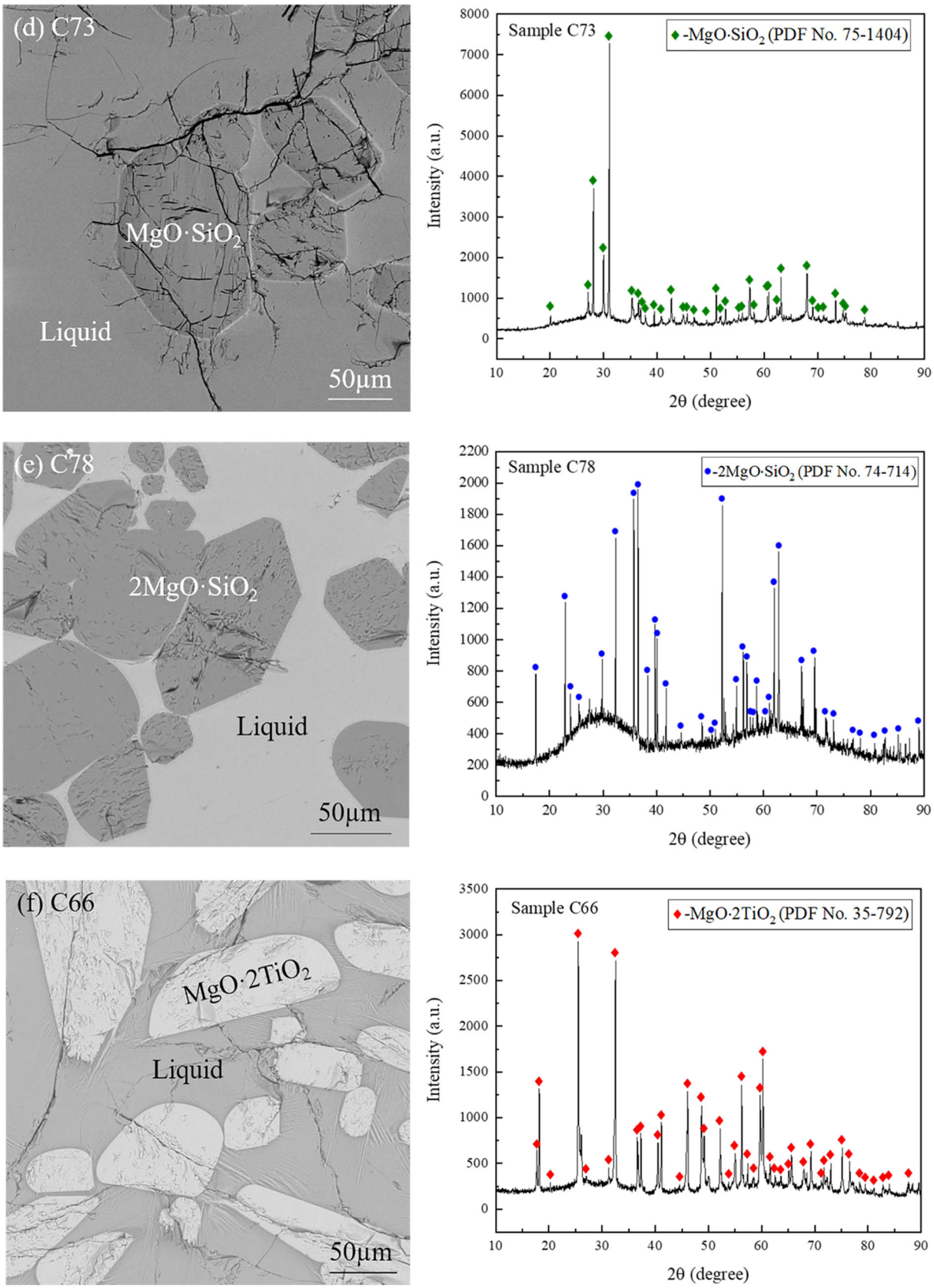

Fig. 3. continued

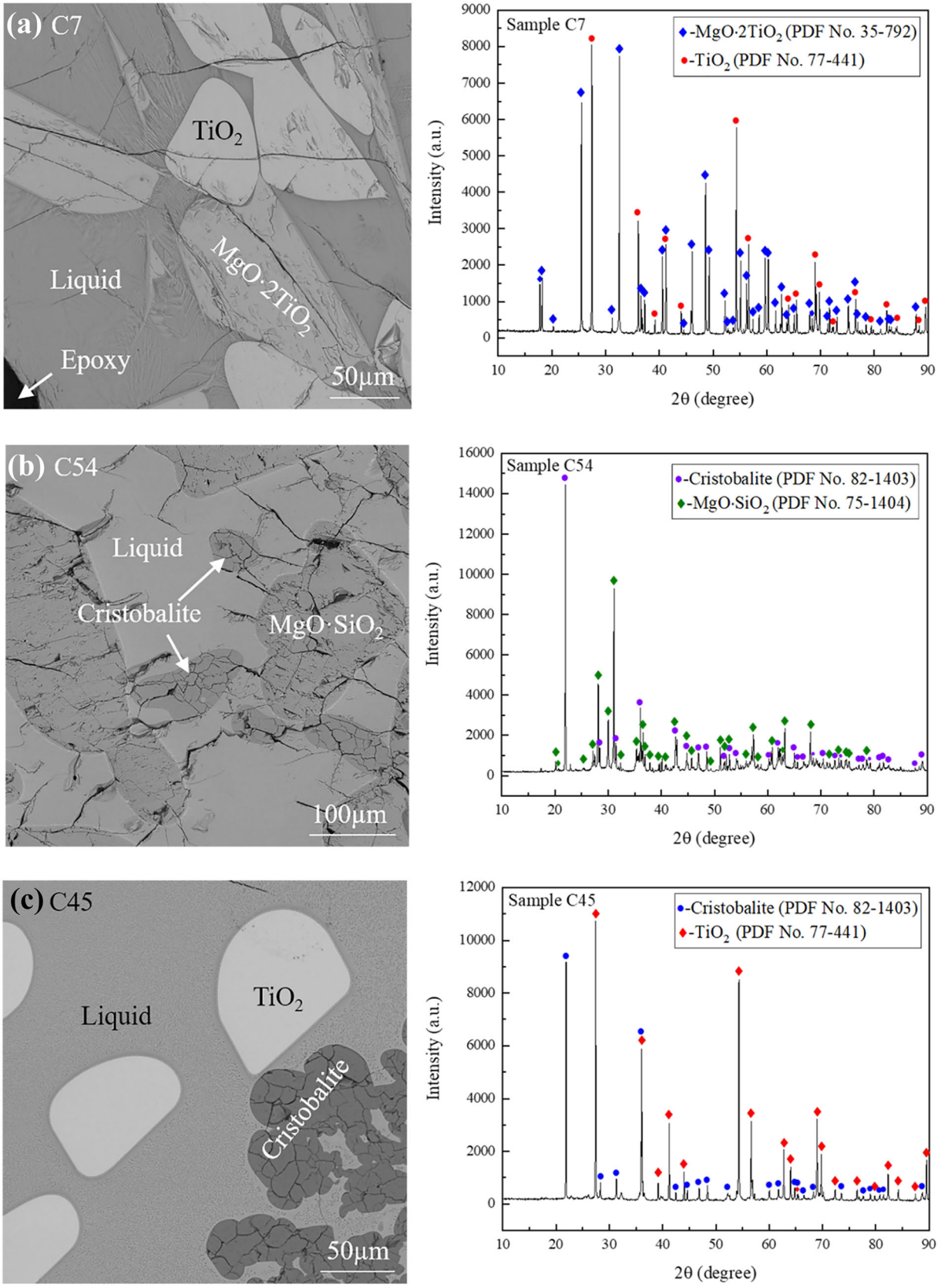

Fig. 4. Back scattered electron images and XRD patterns for liquid-solid-solid three-phase coexisting equilibria; (a) liquid-MgO·2TiO_2-TiO_2; (b) liquid-MgO·SiO_2-cristobalite; (c) liquid-TiO_2-cristobalite; (d) liquid-MgO·SiO_2-2MgO·SiO_2; and (e) liquid-2MgO·SiO_2-MgO·2TiO_2.

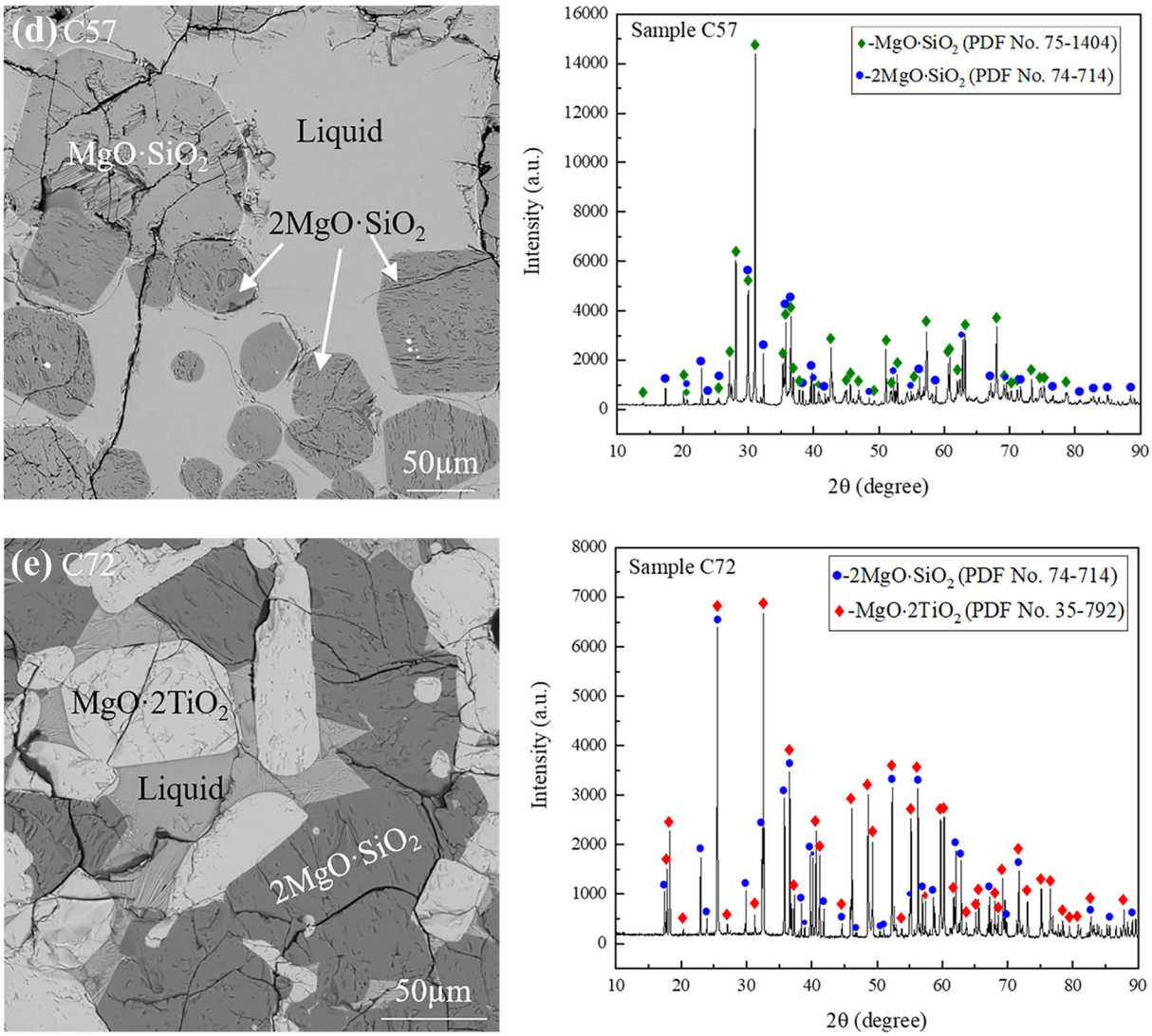

Fig. 4. continued

and experimentally measured TiO_2 composition was found to be lower than 0.3%, indicating the present results measured by EDS are reliable enough for constructing the phase diagram of the SiO_2-MgO-TiO_2 system.

As can be observed in Table II, a certain fraction of TiO_2 was contained in the cristobalite when it was equilibrated with the liquid phase, showing a strong relationship with the TiO_2 concentration of the conjugate liquid phase. Similar observations were reported by Kirschen et al.[83] We plotted the experimentally measured TiO_2 concentrations in cristobalite with the obtained standard deviations as a function of TiO_2 concentration in the liquid oxide phase, see Fig. 5. For some points, the standard deviations were too small to be reproduced. The predictions by MTDATA[84,85] using the Mtox 8.2 database[85] were also plotted in the graph for comparison. As shown in Fig. 5, the lowest experimentally measured TiO_2 concentration in the cristobalite phase did not differ significantly from the prediction by MTDATA. However, the maximum TiO_2 content in the cristobalite phase was approximately 2.5 wt.% lower than the value predicted by MTDATA. Furthermore, the minimum and maximum TiO_2 solubilities in the liquid phase calculated by MTDATA were around 4 wt.% and 5 wt.% lower than the present experimental results, respectively.

The liquid-solid-solid three-phase equilibria observed in the present work can be further analyzed by the Gibbs phase rule,[86] described by Eq. 1:

$$f = C - P + 2 \quad (1)$$

where f refers to the degrees of freedom, and C and P refer to the number of independent components and equilibrium phases, respectively. The number 2 refers to the temperature and total pressure

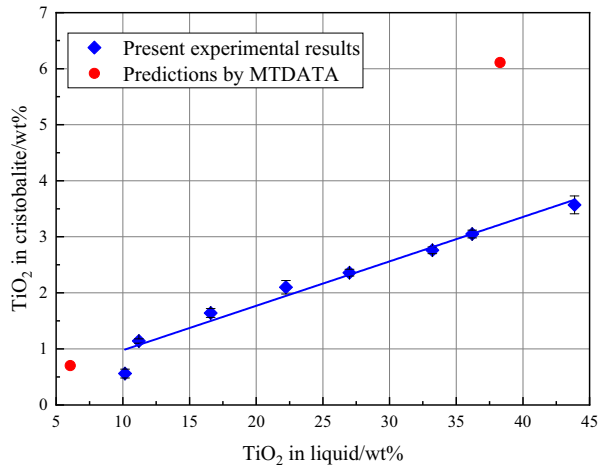

Fig. 5. Concentration of TiO_2 in cristobalite phase versus TiO_2 in liquid oxide.

variables. As the present study was carried out at a fixed temperature and atmospheric pressure with P = 1 atm in air, Eq. 1 can be further simplified as Eq. 2:

$$f = C - P \quad (2)$$

According to the Gibbs phase rule, there could be a maximum of 3 phases coexisting in the MgO-SiO_2-TiO_2 ternary system (f = 0, C = 3, then P = 3) under the present experimental conditions. Therefore, the liquid composition of the liquid-solid-solid three-phase equilibrium was constrained to an invariant point in the MgO-SiO_2-TiO_2 ternary system. The liquid-TiO_2-MgO·2TiO_2 three-phase equilibrium was confirmed in samples C7 and C11; the liquid-cristobalite-MgO·SiO_2 equilibrium was determined in samples C52, C54, and C55. Thus, the invariant point for the liquid oxide-TiO_2-MgO·2TiO_2 coexisting equilibrium was determined by using the average of samples C7 and C11, giving a composition of 50.8 wt.% TiO_2-26.8 wt.% SiO_2-22.4 wt.% MgO for the liquid oxide. Similarly, the invariant point for the liquid oxide-cristobalite-MgO·SiO_2 coexisting equilibrium was calculated as the average of C52, C54, and C55, which produced 9.8 wt.% TiO_2-58.4 wt.% SiO_2-31.8 wt.% MgO.

Construction of the 1500°C Isothermal Phase Diagram

Based on the present experimental data listed in Table II, a 1500°C isothermal section of the MgO-SiO_2-TiO_2 system was constructed, as shown in Fig. 6a. The primary phase fields of cristobalite and MgO·SiO_2 were experimentally determined, and the liquid-cristobalite-MgO·SiO_2 three-phase coexisting equilibrium was observed in this study, thus the phase domain for liquid-cristobalite-MgO·SiO_2 coexisting equilibrium can be constructed by connecting the solid composition points of cristobalite and MgO·SiO_2, and subsequently forming another triangular region #12 for SiO_2-cristobalite-MgO·SiO_2 three-phase coexisting equilibrium. The area marked with a light gray color was not investigated due to the limited number of experimental points. Data from the literature[72] and the simulations by FactSage using the FactPS and FToxid databases[87,88] and by MTDATA using the Mtox 8.2 database[85] were compared with the present results. The results from the literature[72] as well as the calculated liquid oxide domains are shown in Figs. 6b–d.

We found that the experimentally determined isotherm for the cristobalite primary phase field, shown in Fig. 6b, agreed in general with the results by Massazza and Sirchia.[72] However, the present results in the TiO_2 primary phase field shifted slightly to the region with higher TiO_2 content when compared with the observation by Massazza and Sirchia.[72] The 2MgO·SiO_2 primary phase field obtained in the present study was much wider than the results in the literature,[72] expanding toward the region of lower TiO_2 content. The liquid-2MgO·SiO_2-MgO·2TiO_2 three-phase invariant point determined in the present study shows a composition with relatively low TiO_2 and high SiO_2 concentrations. The results for the MgO·SiO_2 primary phase field in the present study are narrower than those found by Massazza and Sirchia,[72] whose results covered significantly wider ranges of SiO_2 and TiO_2 content than the present study.

Figure 6c shows a comparison of the present results with the calculations made by FactSage. The liquid oxide domain determined in this study was much smaller than that calculated by FactSage. The primary phase field of 2MgO·SiO_2 according to FactSage was wider than the present results, expanding toward both the higher and lower TiO_2 content regions. The present isotherm for the MgO·SiO_2 primary phase field shifted slightly to the area with higher TiO_2 content. The isotherms for the TiO_2 and MgO·2TiO_2 primary phase fields measured in this study exhibited lower TiO_2 content but higher SiO_2 concentration than the predictions by FactSage.

Figure 6d shows a comparison of the present results with the simulations by MTDATA. The liquid domain simulated by MTDATA is larger than that of the present results. The isotherm for the MgO·SiO_2 primary phase field obtained in this study displayed a higher TiO_2 content compared with the results by MTDATA. The present results in the cristobalite primary phase field generally agreed well with the predictions by MTDATA in the lower TiO_2 content region, but the present experimentally measured liquid-cristobalite-TiO_2 three-phase invariant point showed a higher TiO_2 content. The isotherm constructed in the MgO·2-TiO_2 primary phase field in the present study shifted to a higher SiO_2 content area with a similar

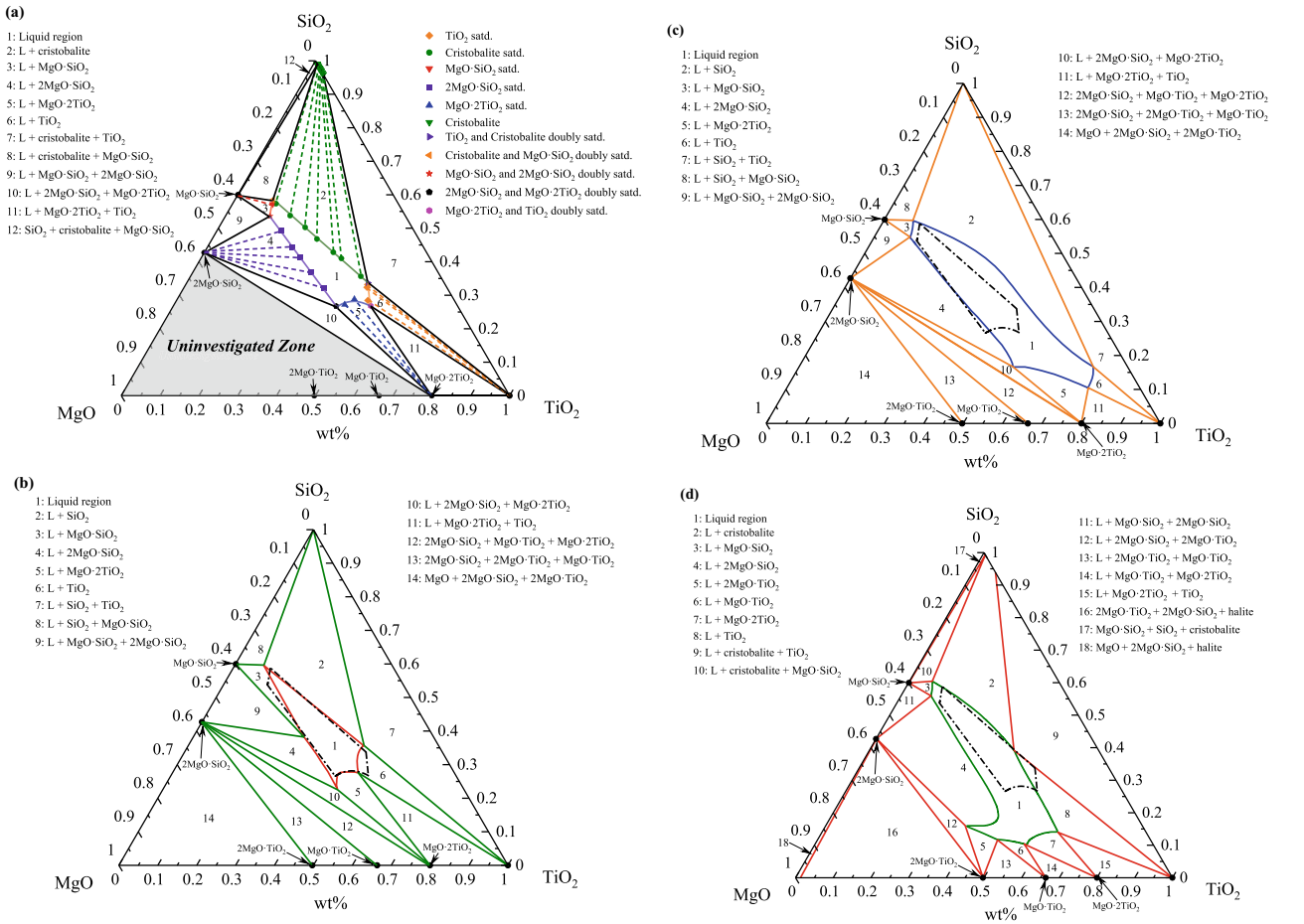

Fig. 6. Isothermal phase diagram of MgO-SiO_2-TiO_2 system in air at 1500°C (a), comparisons of the present results with the data by Massazza and Sirchia [72] (b) in air, and simulations by FactSage (c), and MTDATA (d).

trend to the behavior simulated by MTDATA. The present experimental results of the primary phase field of $2MgO{\cdot}SiO_2$ showed a lower MgO content. However, the primary phase fields of $MgO{\cdot}TiO_2$ and $2MgO{\cdot}TiO_2$ predicted by MTDATA were not observed in the present study.

SUMMARY AND CONCLUSION

The phase equilibria of the SiO_2-MgO-TiO_2 system were investigated at 1500°C in air using the high-temperature isothermal equilibration/quenching/SEM-EDS/XRD analysis technique. We determined the isotherms for the cristobalite, $MgO{\cdot}SiO_2$, $2MgO{\cdot}SiO_2$, $MgO{\cdot}2TiO_2$, and TiO_2 primary phase field.

Based on the experimental results, we generated a 1500°C isothermal section for the SiO_2-MgO-TiO_2 system. We compared the present results with the available data from the literature and with simulations by FactSage and MTDATA. The present results in the cristobalite primary phase field agreed well with the observations in the literature, but showed strong discrepancies in the primary phase fields of $MgO{\cdot}SiO_2$ and TiO_2. The present results provide useful thermodynamic information for the selective crystallization of TiO_2 and $MgO{\cdot}2TiO_2$ phases from the titania-bearing slags by adjusting their compositions. The simulated data by FactSage and MTDATA deviated significantly from the present results. The current experimentally measured data provide guidelines for updating the titania-bearing thermodynamic databases of FactSage and MTDATA thermodynamic software and fundamental information on thermodynamic modeling of more complicated high-order titania systems.

ACKNOWLEDGEMENTS

This work was partly financed by the Aalto University School of Chemical Engineering. The Academy of Finland's RawMatTERS Finland Infrastructure (RAMI) based at Aalto University, GTK Espoo, and VTT Espoo was utilized in this study. The authors are grateful to the China Scholarship Council for financial support [Grant Number 201806370217, 201706370096]. This study received financial support from the Project funded by China Postdoctoral Science Foundation [Grant

Number 2020TQ0059, 2020M680967] and the Natural Science Foundation of Liaoning Province. Mr. Junmo Jeon is greatly appreciated for his assistance in XRD analyses. The authors declare that they have no conflict of interest.

FUNDING

Open access funding provided by Aalto University.

OPEN ACCESS

REFERENCES

1. L. Zhang, W. Zhang, J. Zhang, and G. Li, *Metals* 6, 105. (2016).
2. S. Ren, Q. Zhao, L. Yao, and Q. Liu, *Cryst. Eng. Comm.* 18, 1393. (2016).
3. J. Han, J. Zhang, J. Zhang, X. Chen, L. Zhang, and G. Tu, *ACS Omega* 5, 8619. (2020).
4. Q.Y. Huang, X.W. Lv, R. Huang, and J.J. Song, *Can. Metall. Q.* 52, 413. (2013).
5. Y.L. Zhen, G.H. Zhang, and K.C. Chou, *Metall. Res. Technol.* 113, 507. (2016).
6. Y.L. Zhen, G.H. Zhang, and K.C. Chou, *High Temp. Mater. Processes* 35, 309. (2016).
7. Y.Z. Wang, J.L. Zhang, Z.J. Liu, and C.B. Du, *JOM* 69, 2397. (2017).
8. G.H. Zhang, and K.F. Wang, *Can. Metall. Q.* 57, 80. (2018).
9. L. Zhang, L.N. Zhang, M.Y. Wang, G.Q. Li, and Z.T. Sui, *Miner. Eng.* 20, 684. (2007).
10. L. Wang, W. Liu, J. Hu, Q. Liu, H. Yue, B. Liang, G. Zhang, D. Luo, H. Xie, and C. Li, *Chin. J. Chem. Eng.* 26, 583. (2018).
11. F. Valighazvini, F. Rashchi, and R.K. Nekouei, *Ind. Eng. Chem. Res.* 52, 1723. (2013).
12. H. Jiao, D. Tian, S. Wang, J. Zhu, and S. Jiao, *J. Electrochem. Soc.* 164, D511. (2017).
13. Y. Zhang, *Can. Metall. Q.* 53, 440. (2014).
14. K. Chen, Y. Li, X. Meng, L. Meng, and Z. Guo, *Ceram. Int.* 45, 24236. (2019).
15. S. He, H. Sun, D. Tan, and T. Peng, *Proc. Environ. Sci.* 31, 977. (2016).
16. T. Jiang, H. Dong, Y. Guo, G. Li, and Y. Yang, *Trans. Inst. Min. Metall. Sect. C* 119, 33. (2010).
17. X. Liu, G. Gai, Y. Yang, Z. Sui, L. Li, and J. Fu, *J. China Univ. Min. Technol.* 18, 275. (2008).
18. M. Wu, H. Lü, M. Liu, Z. Zhang, X. Wu, W. Liu, P. Wang, and L. Li, *Hydrometallurgy* 167, 8. (2017).
19. W. Zhang, L. Zhang, J.H. Zhang, and N.X. Feng, *Ind. Eng. Chem. Res.* 51, 12294. (2012).
20. J. Li, Z. Zhang, M. Zhang, M. Guo, and X. Wang, *Steel Res. Int.* 82, 607. (2011).
21. J. Li, X. Wang, and Z. Zhang, *ISIJ Int.* 51, 1396. (2011).
22. L. Zhang, J.H. Zhang, W. Zhang, and G.Q. Li, *Ind. Eng. Chem. Res.* 52, 4924. (2013).
23. W. Zhang, L. Zhang, J.H. Zhang, and N.X. Feng, *Adv. Mater. Res.* 641, 363. (2013).
24. Z. Wang, X. Liu, L. Zhang, and Q. Zhu, *Trans. Indian Inst. Met.* 69, 97. (2016).
25. X.D. Wang, Y.W. Mao, X.Y. Liu, and Y.K. Zhu, *J. Iron Steel Res. Int.* 3, 1. (1990).
26. Y. Sun, J. Li, X. Wang, and Z. Zhang, *Metall. Mater. Trans. B* 45B, 1446. (2014).
27. L. Sun, J. Shi, Z. Yu, and M. Jiang, *Ceram. Int.* 45, 481. (2019).
28. W. Zhang, L. Zhang, Y. Li, and X. Li, *Green Process. Synth.* 4, 307. (2015).
29. E.F. Osborn, and K.H. Gee, *Bull. Earth Mineral. Sci. Expt. Stn.* 85, 57. (1969).
30. B. Zhao, E. Jak, and P.C. Hayes, *VIII International Conference on Molten Slags, Fluxes and Salts*, Santiago, Chile. ChIMM, Santiago, 71 (2009).
31. Goso X, Nell J, and Petersen J, ed. R.G. Reddy, P. Chaubal, P.C. Pistorius, U. Pal, Advances in Molten Slags, Fluxes, and Salts: *Proceedings of the 10th International Conference on Molten Slags, Fluxes and Salts 2016*. Springer, Cham, 105, 2016.
32. M. Chen, J. Shi, P. Taskinen, and A. Jokilaakso, *Ceram. Int.* 46, 27702. (2020).
33. J. Shi, M. Chen, X. Wan, P. Taskinen, and A. Jokilaakso, *JOM* 72, 3204. (2020).
34. J. Shi, M. Chen, I. Santoso, L. Sun, M. Jiang, P. Taskinen, and A. Jokilaakso, *Ceram. Int.* 46, 1545. (2020).
35. Z. Wang, Q. Zhu, and H. Sun, *Metall. Mater. Trans. B* 50B, 357. (2019).
36. J. Shi, L. Sun, J. Qiu, and M. Jiang, *ISIJ Int.* 58, 431. (2018).
37. J. Shi, L. Sun, J. Qiu, and M. Jiang, *J. Alloys Compd.* 722, 25. (2017).
38. J. Shi, L. Sun, B. Zhang, X. Liu, J. Qiu, Z. Wang, and M. Jiang, *Metall. Mater. Trans. B* 47B, 425. (2016).
39. J. Shi, L. Sun, J. Qiu, Z. Wang, B. Zhang, and M. Jiang, *ISIJ Int.* 56, 1124. (2016).
40. L. Sun, J. Shi, C. Liu, and M. Jiang, *J. Alloys Compd.* 810, 151949. (2019).
41. L.F. Sun, J.J. Shi, B. Zhang, J.Y. Qiu, Z.Y. Wang, M.F. Jiang, and J. Cent, *South Univ.* 24, 48. (2017).
42. M. T. Kirschen, Immiscible silicate melts in the system CaO-MgO-SiO_2-TiO_2-Al_2O_3. *PhD dissertation*, 1998, Basel University.
43. Z. Wang, H. Sun, L. Zhang, and Q. Zhu, *J. Alloys Compd.* 671, 137. (2016).
44. M. Chen, J. Shi, P. Taskinen, and A. Jokilaakso, *Ceram. Int.* 46, 9183. (2020).
45. A. Jongejan, and A.L. Wilkins, *J. Less Common Met.* 20, 273. (1970).
46. W. Gong, L. Wu, and A. Navrotsky, *J. Am. Ceram. Soc.* 101, 1361. (2018).
47. I. Shindo, *J. Cryst. Growth* 50, 839. (1980).
48. F. Massazza, and E. Sirchia, *Chim. Ind.* 40, 376. ((**In Italian**)) (1958).
49. E. Woermann, B. Brezney, and A. Muan, *Am. J. Sci.* 267, 463. (1969).
50. G. Eriksson, and A.D. Pelton, *Metall. Trans. B* 24B, 795. (1993).
51. R. DeVries, R. Roy, and E. Osborn, *Trans. Br. Ceram. Soc.* 53, 525. (1954).
52. E.N. Bunting, *Bur. Stand. J. Res.* 11, 719. (1933).
53. R.W. Ricker, and F.A. Hummel, *J. Am. Ceram. Soc.* 34, 271. (1951).
54. S.A. Kirillova, V.I. Almjashev, and V.V. Gusarov, *Russ. J. Inorg. Chem.* 56, 1464. (2011).
55. C. DeCapitani, and M. Kirschen, *Geochim. Cosmochim. Acta* 62, 3753. (1998).

56. S.M. Lang, C.L. Fillmore, and L.H. Maxwell, *J. Res. Natl. Bur. Stand.* 48, 298. (1952).
57. I.H. Jung, G. Eriksson, P. Wu, and A. Pelton, *ISIJ Int.* 49, 1290. (2009).
58. M. Ilatovskaia, G. Savinykh, and O. Fabrichnaya, *J. Phase Equilib. Diffus.* 38, 175. (2017).
59. K. Das, P. Choudhury, and S. Das, *J. Phase Equilib.* 23, 525. (2002).
60. M.H. Berger, and A. Sayir, *J. Eur. Ceram. Soc.* 28, 2411. (2008).
61. R.C. DeVries, R. Roy, and E.F. Osborn, *J. Am. Ceram. Soc.* 38, 158. (1955).
62. G. Ye, and T. Rosenqvist, *Scand. J. Metall.* 20, 222. (1991).
63. V. Daněk, and I. Nerád, *Chem. Pap.* 56, 241. (2002).
64. X. Wan, J. Shi, L. Klemettinen, M. Chen, P. Taskinen, and A. Jokilaakso, *J. Alloys Compd.* 847, 156472. (2020).
65. J.A. Imlach, and F.P. Glasser, *Trans. Br. Ceram. Soc.* 67, 581. (1968).
66. S. Ueda, K. Takemoto, T. Ikeda, and M. Maeda, *ISIJ Int.* 40, S92. (2000).
67. M.A. Rouf, A.H. Cooper, and H.B. Bell, *Trans. Br. Ceram. Soc* 68, 263. (1969).
68. Verein Deutsche Eisenhüttenleute, *Slag Atlas*, 2nd edn. (Verlag Stahleisen GmbH, Düsseldorf, 1995).
69. M. Kirschen, C. DeCapitani, F. Millot, J.C. Rifflet, and J.P. Coutures, *Eur. J. Mineral.* 11, 427. (1999).
70. M. Ilatovskaia, I. Saenko, G. Savinykh, and O. Fabrichnaya, *J. Am. Ceram. Soc.* 101, 5198. (2018).
71. M. Ilatovskaia, and O. Fabrichnaya, *J. Alloys Compd.* 790, 1137. (2019).
72. F. Massazza, and E. Sirchia, *Chim. Ind. (Milan)* 40, 460. ((**In Italian**)) (1958).
73. I.D. MacGregor, *Am J Sci A* 267, 342. (1969).
74. J. Hermann, H.S.C. O'Neill, and A.J. Berry, *Contrib. Mineral. Petrol.* 148, 746. (2005).
75. B. Yan, X. Wang, and Z. Yang, *J. Alloys Compd.* 695, 3476. (2017).
76. E. Jak, and P.C. Hayes, *Miner. Process. Extr. Metall.* 117, 1. (2008).
77. E. Jak and P.C. Hayes, *VII International Conference on Molten Slags Fluxes and Salts*, Cape Town, SAIMM, Johannesburg, 85 (2004).
78. G.F. Bastin, J.M. Dijkstra, and H.J.M. Heijligers, *X Ray Spectrom.* 27, 3. (1998).
79. P.J. Mackey, *Can. Metall. Q.* 21, 221. (1982).
80. B. Keyworth, *6th International Precious Metals Institute*, California, Pergamon, 509 (1983).
81. X. Wan, M. Chen, Y. Qiu, J. Shi, J. Li, C. Liu, P. Taskinen, and A. Jokilaakso, *Ceram. Int.* 47, 11176. (2021).
82. X. Wan, J. Shi, Y. Qiu, M. Chen, J. Li, C. Liu, P. Taskinen, and A. Jokilaakso, *Ceram. Int.* https://doi.org/10.1016/j.ceramint.2021.05.205 (2021).
83. M. Kirschen, and C. DeCapitani, *J. Phase Equilib.* 20, 593. (1999).
84. R.H. Davies, A.T. Dinsdale, J.A. Gisby, J.A.J. Robinson, and A.M. Martin, *Calphad* 26, 229. (2002).
85. J. Gisby, P. Taskinen, J. Pihlasalo, Z. Li, M. Tyrer, J. Pearce, K. Avarmaa, P. Björklund, H. Davies, M. Korpi, S. Martin, L. Pesonen, and J. Robinson, *Metall. Mater. Trans. B* 48B, 91. (2017).
86. M. Zhao, L. Song, and X. Fan, *The Boundary Theory of Phase Diagrams and its Application* (Science Press, Beijing, 2009).
87. C.W. Bale, E. Bélisle, P. Chartrand, S.A. Decterov, G. Eriksson, K. Hack, I.H. Jung, Y.B. Kang, J. Melançon, A.D. Pelton, C. Robelin, and S. Petersen, *Calphad* 33, 295. (2009).
88. I.H. Jung, and M.A. Van Ende, *Metall. Mater. Trans. B* 51B, 1851. (2020).